Original Article

ZNF528 as a novel driver of metastasis in lung cancer: insights from single-cell transcriptomics

Huiying Li[1,2], Yongjuan Lin[2], Yue Wang[3], Xin Chen[3], Yu Xie[2], Tingting Yu[2], Jian He[4], Zhenyu Yin[3], Mao Xia[1]

[1]Department of Clinical Laboratory Medicine, The Affiliated Hospital of Nantong University, Nantong, China; [2]Department of Geriatric Oncology, Affiliated Nanjing Drum Tower Hospital of Nanjing University Medical School, Nanjing, China; [3]Department of Geriatrics Oncology, Nanjing Drum Tower Hospital Clinical College of Nanjing University of Chinese Medicine, Nanjing, China; [4]Department of Nuclear Medicine, Affiliated Nanjing Drum Tower Hospital of Nanjing University Medical School, Nanjing, China

Contributions: (I) Conception and design: M Xia, Z Yin, J He; (II) Administrative support: M Xia, Z Yin, J He; (III) Provision of study materials or patients: H Li; (IV) Collection and assembly of data: H Li; (V) Data analysis and interpretation: H Li, Y Lin, Y Wang, X Chen, Y Xie, T Yu; (VI) Manuscript writing: All authors; (VII) Final approval of manuscript: All authors.

Correspondence to: Mao Xia, MD, PhD. Department of Clinical Laboratory Medicine, The Affiliated Hospital of Nantong University, No. 20 Xisi Road, Nantong 226001, China. Email: xiamao@ntu.edu.cn; Zhenyu Yin, MD, PhD. Department of Geriatrics Oncology, Nanjing Drum Tower Hospital Clinical College of Nanjing University of Chinese Medicine, No. 138 Xianlin Road, Nanjing 210023, China. Email: zhenyuyin@njglyy.com; Jian He, MD, PhD. Department of Nuclear Medicine, Affiliated Nanjing Drum Tower Hospital of Nanjing University Medical School, No. 321 Zhongshan Road, Nanjing 210008, China. Email: karina_lee@126.com.

Background: Non-small cell lung cancer (NSCLC) remains a leading cause of cancer mortality due to frequent metastasis, despite therapeutic advances. This study aims to identify novel drivers of NSCLC metastasis to facilitate the development of prognostic biomarkers and therapeutic targets.

Methods: We analyzed single-cell RNA-seq data (GSE121907) to identify differentially expressed genes (DEGs) in epithelial cells from metastatic NSCLC. Functional enrichment was performed. Based on bioinformatic findings, we investigated the role of zinc finger protein 528 (*ZNF528*) through gain- and loss-of-function studies in NSCLC cell lines. Cellular proliferation, migration, and invasion were assessed using Cell Counting Kit-8 (CCK-8), wound healing, and Transwell assays, respectively. Epithelial-mesenchymal transition (EMT) markers were analyzed by immunoblotting. A cell-derived xenograft (CDX) model was established to evaluate tumor growth and metastasis *in vivo*.

Results: Single-cell analysis revealed an expanded epithelial compartment in metastatic samples. Among the DEGs identified in these epithelial cells, *ZNF528* was significantly upregulated. Pathway analysis indicated enrichment of *ZNF528*-correlated genes in proliferation and invasion-related pathways (e.g., NF-κB, MAPK). Consistently, functional assays demonstrated that *ZNF528* knockdown suppressed, while its overexpression enhanced, NSCLC cell proliferation, migration, invasion, and EMT *in vitro*. Moreover, *ZNF528* overexpression promoted tumor growth and metastasis in mouse xenograft models.

Conclusions: *ZNF528* acts as a novel promoter of NSCLC metastasis, representing a potential prognostic biomarker and therapeutic target.

Keywords: Non-small cell lung cancer (NSCLC); metastasis; zinc finger protein 528 (*ZNF528*); epithelial-mesenchymal transition (EMT); single-cell RNA sequencing (scRNA-seq)

Submitted Jan 04, 2026. Accepted for publication Apr 14, 2026. Published online May 26, 2026.
doi: 10.21037/tlcr-2026-1-0008
View this article at: https://dx.doi.org/10.21037/tlcr-2026-1-0008

Introduction

Lung cancer ranks among the most prevalent cancers and is the leading cause of cancer-related mortality worldwide. It was estimated that in 2022, there were approximately 2.5 million new cases and over 1.8 million deaths globally (1). Non-small cell lung cancer (NSCLC), which accounts for about 85% of all lung cancer cases, primarily includes lung adenocarcinoma (LUAD), lung squamous cell carcinoma (LUSC), and large cell carcinoma (2). Despite recent therapeutic advances, the 5-year survival rate for NSCLC patients remains poor (10–20%) (3), largely due to tumor metastasis and invasion—key factors contributing to treatment failure (4). However, the molecular mechanisms underlying NSCLC metastasis are not yet fully understood. Thus, elucidating these mechanisms is critical for developing more effective metastatic biomarkers and potential therapeutic targets.

In recent years, high-throughput single-cell RNA sequencing (scRNA-seq) has greatly advanced the characterization of tumor biology and facilitated the discovery of therapeutic targets, including in lung cancer. Utilizing this technology, we identified elevated expression of zinc finger protein 528 (ZNF528) in lung cancer. ZNF528 belongs to the KRAB C2H2 zinc finger protein family, the largest family of transcription factors in humans (5). Members of this family typically function as transcriptional repressors and are involved in diverse biological processes such as embryonic development, apoptosis, oncogenic transformation, cell cycle regulation, and the control of cell differentiation and proliferation (6). These proteins bind DNA through their zinc finger domains, while the KRAB domain interacts with KRAB-associated protein 1 (KAP1) to recruit additional co-regulators (7-9). In addition to DNA binding, the zinc finger structural domain is involved in protein-protein interactions (10). *ZNF528* has a variety of biological roles and is a regulator of bone-related biological functions, and its mutation affects the expression of osteoporosis-related genes (11). However, its role in cancer remains largely unexplored, with limited literature available on its molecular function. One study employing RNA sequencing reported that wild-type *ZNF528* regulates cell cycle and cancer-related signaling pathways, whereas a *ZNF528* mutant upregulates the Wnt and Notch signaling pathways (11). The Wnt signaling pathway plays key roles in cell cycle progression, cell death, epithelial-mesenchymal transition (EMT), angiogenesis, stemness, and the tumor immune microenvironment. Its dysregulation is associated with various cancers and contributes to tumor initiation, progression, metastasis, and drug resistance (12-14). Similarly, the Notch signaling pathway has been implicated in tumorigenesis, progression, metastasis, and chemoresistance (15,16), suggesting a potential role for *ZNF528* in lung cancer progression. In this study, we aimed to investigate the molecular mechanisms of lung cancer metastasis using single-cell sequencing. We analyzed scRNA-seq data from primary and metastatic lung cancer samples obtained from the Gene Expression Omnibus (GEO) database. By examining the expression profiles of differentially expressed genes (DEGs) in epithelial cells, we identified *ZNF528* as upregulated in metastatic lung cancer tissues. *ZNF528* may thus serve as a prognostic indicator and diagnostic marker for lung cancer metastasis. Through *in vitro* and *in vivo* experiments, we further demonstrated that *ZNF528* promotes lung cancer cell migration and invasion by facilitating EMT. We present this article in accordance with the ARRIVE and MDAR reporting checklists (available at https://tlcr.amegroups.com/article/view/10.21037/tlcr-2026-1-0008/rc).

Highlight box

Key findings

- Single-cell RNA sequencing of human NSCLC revealed zinc finger protein 528 (ZNF528) as a significantly upregulated gene in metastatic epithelial cells, and its high expression correlated with poor prognosis in clinical cohorts.
- ZNF528 promoted NSCLC cell proliferation, migration, invasion, and epithelial-mesenchymal transition (EMT) *in vitro*, at least in part through a SNAIL-dependent mechanism and activation of Wnt/Notch signaling.
- ZNF528 overexpression enhanced tumor growth and lung metastasis in mouse xenograft models, accompanied by EMT marker changes *in vivo*.

What is known and what is new?

- Metastasis is the major cause of NSCLC-related death, yet its molecular drivers remain incompletely understood. ZNF528, a KRAB-C2H2 zinc finger protein, has known roles in bone biology but is largely uncharacterized in cancer.
- This study provides the first evidence that ZNF528 is overexpressed in metastatic NSCLC epithelium, promotes metastasis via SNAIL-mediated EMT and Wnt/Notch pathway activation, and holds prognostic value.

What is the implication, and what should change now?

- ZNF528 represents a novel prognostic biomarker and therapeutic target for metastatic NSCLC.
- Future research should validate ZNF528 in larger clinical cohorts and explore strategies to block ZNF528-driven signaling for metastasis prevention and therapy.

Methods

Bioinformatics analyses

Data acquisition and processing

Datasets for this study were obtained from public repositories. The scRNA-seq dataset GSE131907 was downloaded from the GEO (https://www.ncbi.nlm.nih.gov/geo/). Bulk RNA-seq data for LUAD were retrieved from the GEO database using the NSCLC cohort GSE31210, which provides transcriptome expression profiles and corresponding clinical follow-up information. This cohort comprises a total of 226 LUAD samples, with molecular subtypes including *EGFR* mutations (127 cases), *KRAS* mutations (20 cases), *EML4-ALK* fusion (11 cases), and triple-negative cases (68 cases).

scRNA-seq data processing and analysis

The scRNA-seq data were processed and analyzed using the Seurat package (version 4.0). Quality control was performed by retaining cells that expressed more than 200 genes and had a total RNA count (nCount_RNA) between 200 and 50,000. Genes detected in at least 5 cells were included for downstream analysis. After filtering, 20,665 cells from the metastatic lymph node (mLN) group and 43,721 cells from the primary lung (tLung) group were retained for subsequent analysis. The top 5,000 highly variable genes were selected for dimensionality reduction. Principal component analysis (PCA) was performed, followed by clustering using a shared nearest neighbor (SNN) algorithm, which identified 24 distinct cell clusters. Uniform Manifold Approximation and Projection (UMAP) was applied for visualization. Based on the dimensionality reduction results, a nearest-neighbour graph was constructed using FindNeighbors () (dims =1:30), and clustering was performed using the FindClusters () function across a range of resolutions (0–1, in increments of 0.1). A clustering stability tree was generated using the Clustree package, and the most stable resolution (0.5) was selected as the final clustering level.

Cell type annotation and marker identification

Cell types were annotated automatically using the SingleR package with the BlueprintEncodeData reference, identifying eight major cell types: T cells, NK cells, myeloid cells, B cells, mast cells, fibroblasts, epithelial cells, and endothelial cells. Marker genes for each cell type were identified using the 'FindAllMarkers' function in Seurat, which employs a Wilcoxon rank-sum test.

Epithelial cell sub-analysis

Epithelial cells were extracted for further investigation. Differential gene expression between the mLN and tLung epithelial populations was assessed using the 'FindMarkers' function, with DEGs defined as those with an adjusted $P<0.05$ and $|\log_2 \text{fold change}| >1$. Epithelial cells were then re-clustered into 13 subgroups (EC0–EC12). Pseudotime trajectory analysis was performed on all epithelial cells using Monocle2.

Functional enrichment analysis

Functional enrichment analysis was performed using the clusterProfiler (v4.12.6), enrichplot (v1.24.0), org.Hs.eg.db (v3.19.1), topGO (v2.56.0), and GO.db (v3.19.1) packages. Gene Ontology (GO) and Kyoto Encyclopedia of Genes and Genomes (KEGG) analyses were conducted to identify biological processes and signalling pathways associated with DEGs. In addition, gene set enrichment analysis (GSEA) was performed using clusterProfiler combined with Hallmark and KEGG gene sets provided by msigdbr (v2023.1.1). Enrichment results were visualised using enrichplot, ggplot2, and ComplexHeatmap (v2.20.0), and enrichment network circular plots were generated using circlize (v0.4.16).

Bulk RNA-seq analysis of GSE31210

The transcriptome expression profiles and corresponding clinical follow-up information of the NSCLC cohort GSE31210 were downloaded from the GEO database. This cohort consisted of a total of 226 LUAD samples, with molecular subtypes including *EGFR* mutations (127 cases), *KRAS* mutations (20 cases), *EML4-ALK* fusion (11 cases), and triple-negative cases (68 cases). To ensure the accuracy of prognostic analysis, all 226 samples with follow-up time greater than 0 were included in subsequent survival modeling.

Prognostic grouping and survival analysis

To evaluate the clinical prognostic value of *ZNF528* in LUAD, patients were divided into *ZNF528* high-expression and low-expression groups based on the median messenger RNA (mRNA) expression level of *ZNF528* in this cohort.

The Kaplan-Meier (K-M) survival curve was used to illustrate the differences in cumulative survival probability between the two groups during the follow-up period. The Log-rank test was employed to assess the statistical significance of the difference in survival curves between the

expression groups.

Experimental validation

Clinical tissue samples

A total of 60 paired primary (NSCLC tissues and matched adjacent non-tumor lung tissues (≥5 cm from the tumor margin) were collected from patients who underwent surgical resection at Nanjing Drum Tower Hospital. Due to inevitable tissue loss during the preparation and staining processes, 59 adjacent non-tumor samples and 56 tumor tissues were finally available for immunohistochemical (IHC) analysis. All specimens were histologically confirmed by two independent pathologists. The study was conducted in accordance with the Declaration of Helsinki and its subsequent amendments. This study was approved by the Ethics Committee of Nanjing Drum Tower Hospital (approval No. 263-02), and written informed consent was obtained from all patients prior to sample collection.

Cell culture and transfection

The human normal bronchial epithelial cell line BEAS-2B and NSCLC cell lines NCI-H292, HCC827, A549 and NCI-H358 were obtained from the Cell Bank of the Chinese Academy of Sciences. The luciferase-labeled mouse Lewis lung carcinoma (Luc-LLC) cell line was purchased from Shanghai Tianyi Zhonghe Biotechnology Co., Ltd. (Shanghai, China). Cells were cultured in F-12 medium (Gibco, #12634010, Grand Island, NY, USA) or RPMI-1640 medium (Proteintech, #PM00032, Chicago, IL, USA), both supplemented with 10% fetal bovine serum (Corning, #35-081-CV, Corning, NY, USA). *ZNF528*-specific short hairpin RNA (shRNA) oligonucleotides and the *ZNF528* overexpression plasmid were constructed by Shanghai HeYuan Biotechnology Co., Ltd. (Shanghai, China). The targeting shRNA sequence for human *ZNF528* was 5'-CCAGAAGCUGUACAAUCAATT-3'; a non-targeting scrambled shRNA (5'-UUCUCCGAAC GUGUCACGUTT-3') served as a negative control. For transfection, A549 and NCI-H358 cells were seeded and allowed to reach 70–80% confluency, after which shRNA or plasmid was delivered using Lipofectamine™ 8000 (Beyotime, #C0533, Shanghai, China) following the manufacturer's protocol.

Reverse transcription quantitative polymerase chain reaction (RT-qPCR)

Total RNA was extracted using the RNeasy Mini Kit (Qiagen, #74014, Hilden, NRW, Germany) and quantified with a NanoDrop 2000 (Thermo Scientific, Waltham, MA, USA). Complementary DNA (cDNA) was synthesized from 1 µg RNA using SuperScript™ IV VILO™ Master Mix (Thermo Fisher, #11756050, USA). Quantitative polymerase chain reaction (qPCR) was performed in triplicate using SYBR Green PCR Master Mix (Bio-Rad) under the following conditions: 95 ℃ for 3 min; 40 cycles of 95 ℃ for 10 s, 60 ℃ for 30 s, and 72 ℃ for 30 s. Gene expression was normalized to glyceraldehyde-3-phosphate dehydrogenase (GAPDH) and analyzed via the $2^{-\Delta\Delta CT}$ method. Primer sequences: *ZNF528* (F: 5'-GAGGACCTGGAGCAGTTTGA-3'; R: 5'-TGCTGCTCTGTTGCTGTTCT-3'); GAPDH (F: 5'-AGATCCCTCCAAAATCAAGTGG-3'; R: 5'-GGCAGAGATGATGACCCTTTT-3').

Cell proliferation assays

Cells were seeded in 96-well plates at a density of 1×10^4 cells per well and cultured in fresh medium. For each group, five replicate wells were used. Cell viability was assessed at 0, 24, 48, 72, and 96 hours using a Super-Enhanced Cell Counting Kit-8 (CCK-8) (C0048M-500T, Beyotime, Shanghai, China) according to the manufacturer's instructions. Absorbance at 450 nm (A450) was measured using a microplate reader. The entire assay was performed in triplicate.

Cell scratch healing experiment

A549 and NCI-H358 cells were seeded in 6-well plates at 5×10^5 cells per well and grown to approximately 90% confluency. A uniform scratch was made across the cell monolayer using a sterile 200 µL pipette tip. After washing, cells were maintained in serum-free medium. Wound closure was monitored at 0 and 24 hours under a microscope, and images were captured for analysis. The distance between wound edges was measured using ImageJ software, and the migration rate was calculated.

Transwell assay

Cell invasion was evaluated using Transwell chambers (8-µm pore size). The lower chambers were filled with medium containing 10% FBS as a chemoattractant. After serum starvation for 12 hours, 2×10^4 A549 or NCI-H358 cells in serum-free medium were seeded into the upper chambers. Following 24 hours of incubation at 37 ℃, cells that had invaded through the membrane were fixed with absolute ethanol for 20 minutes and stained with 0.1% crystal violet

for another 20 minutes. Non-invading cells on the upper surface were removed with a cotton swab. Stained cells were imaged under a microscope, and the average number of cells per field from at least six random fields was counted to quantify invasion.

Immunoblotting

Total protein was extracted from NSCLC cells, separated by 10% SDS-PAGE, and transferred onto PVDF membranes (PE0010, Millipore, Billerica, MA, USA). Membranes were blocked and then incubated overnight at 4 ℃ with the following primary antibodies: anti-E-cadherin (20874-1-AP, Proteintech, Chicago, IL, USA; 1:5,000), anti-N-cadherin (22018-1-AP, Proteintech; 1:3,000), anti-Vimentin (10366-AP, Proteintech; 1:20,000), anti-SNAI2/SLUG (12129-1-AP, Proteintech; 1:10,000), anti-*ZNF528* (SAB2102898, Merck, Darmstadt, Germany; 1:2,000), anti-GSK-3β (67329-1-Ig, Proteintech; 1:5,000), anti-p-GSK-3β (P00791-2, boster, Pleasanton, CA, USA; 1:5,000), anti-β-catenin (A19657, abclonal, Woburn, MA, USA; 1:5,000), anti-Notch (20687-1-AP, Proteintech; 1:5,000), anti-NICD (20687-1-AP, Proteintech; 1:5,000), anti-Hes1 (A0925, abclonal; 1:5,000) and anti-β-Actin (20536-1-AP, Proteintech; 1:5,000). After washing, membranes were incubated with an HRP-conjugated secondary antibody (GB23303, Servicebio, Wuhan, China; 1:8,000) for 1 hour at room temperature. Protein bands were visualized using enhanced chemiluminescence substrate and imaged with a chemiluminescence detection system.

Animal experiment

Twelve male nude mice (5–6 weeks old, 15–20 g) were obtained from Shanghai Jihui Laboratory Animal Co., Ltd. (Shanghai, China). Experiments were performed under a project license (approval No. 263-02) granted by the Ethics Committee of Nanjing Drum Tower Hospital, in compliance with institutional guidelines for the care and use of animals. To establish a subcutaneous xenograft model, A549 cells transfected with either a *ZNF528* overexpression plasmid or an empty vector control were harvested and resuspended in sterile PBS. Each mouse received a subcutaneous injection of 100 μL cell suspension containing 1×10^7 cells. Mice were randomly divided into two groups (n=6 per group): the *ZNF528* overexpression group and the vector control group. Tumor growth was monitored every three days by measuring tumor dimensions with a caliper. Tumor volume was calculated using the formula: volume = (length × width^2)/2. After 28 days, the mice were humanely euthanized, and the tumors were surgically removed, photographed, and weighed. For further analysis, tumor specimens were preserved by freezing at –80 ℃ or 4% paraformaldehyde fixation.

Experimental metastasis was evaluated using a tail-vein injection model. Luciferase-labeled LLC cells stably overexpressing *ZNF528* or empty vector were injected intravenously (2×10^5 cells/mouse) into nude mice (n=6 per group). Following injection, general health status was monitored through daily observation of diet and body weight. Metastatic progression was assessed via bioluminescence imaging after intraperitoneal administration of D-luciferin. At the experimental endpoint (3 weeks post-injection), lung tissues were harvested, with one lobe snap-frozen for subsequent molecular analysis and the other lobe fixed in paraformaldehyde for histological examination.

Histopathology and immunohistochemistry (IHC)

Tumor samples were fixed overnight in 4% paraformaldehyde at 4 ℃, embedded in paraffin, and sectioned at a thickness of 4 μm. Sections were stained with hematoxylin and eosin (H&E; G1005-500ML, Servicebio) for histopathological evaluation. Three representative sections per group were examined under a light microscope.

For IHC, tissue slides were deparaffinized, rehydrated through a graded alcohol series, and subjected to antigen retrieval in sodium citrate buffer. Endogenous peroxidase activity was blocked with 0.3% H_2O_2, followed by incubation with 1% goat serum for 30 minutes at room temperature. Sections were then incubated overnight at 4 ℃ with a primary antibody against Ki67 (28074-1-AP, Proteintech). Subsequently, slides were incubated with a horseradish peroxidase (HRP)-conjugated secondary antibody for 30 minutes at room temperature. Staining was developed using 3,3'-diaminobenzidine (DAB) as a chromogen, and nuclei were counterstained with hematoxylin.

Statistical analysis

All bioinformatics and statistical analyses were performed using R software (version 4.4.2). Visualizations were generated primarily using the ggplot2 (v3.5.2), ComplexHeatmap (v2.20.0), and circlize (v0.4.16) packages. Specifically, time-related event survival modeling was conducted using the survival (v3.7.0) package, and high-quality Kaplan-Meier curves were plotted using the survminer (v0.4.9) package. For comparisons of continuous variables between two groups, either the Wilcoxon rank

sum test or Student's *t*-test was used, depending on the data distribution. For comparisons among multiple groups, the Kruskal-Wallis test or one-way analysis of variance (ANOVA) was applied. To control for false positives due to multiple comparisons, the Benjamini-Hochberg method was used to adjust P values [false discovery rate (FDR) correction]. All statistical tests were two-sided, and a two-sided P<0.05 was considered statistically significant.

Statistical analyses were performed using GraphPad Prism (version 10.1.2). Continuous data are presented as mean ± standard deviation (SD). Differences between two groups were assessed using two-tailed Student's t-test, while comparisons among more than two groups were analyzed by one-way ANOVA. The Chi-squared test (χ^2 test) was used to compare the distribution of clinicopathological features (gender, age group, tumor grade, distant metastasis, and lymph node metastasis) between the *ZNF528* low-expression and high-expression groups. A P<0.05 was considered statistically significant. Significance levels are indicated in figures as follows: *, P<0.05; **, P<0.01; ***, P<0.001, and ****, P<0.0001.

Results

The single-cell landscape of primary and metastatic lung cancer

scRNA-seq data from 7 human lung cancer lymphatic metastasis samples and 11 primary lung cancer samples were obtained from the GEO dataset GSE131907 for in-depth analysis. Samples were categorized into lung cancer lymphatic metastases (mLN) and primary lung tumors (tLung). Following standard quality control to exclude compromised cells and multiplets, data were processed using the Seurat R package. Cell filtering criteria included: genes detected per cell >200, and total RNA molecules per cell (nCount_RNA) between 200 and 50,000 (Figure S1A). After quality filtering, 20,665 cells from the mLN group and 43,721 cells from the tLung group were retained for downstream analysis. The optimal number of principal components for subsequent analysis was determined using an elbow plot (Figure S1B).

Cells from both the mLN and tLung groups were subjected to two-step dimensionality reduction, first with PCA and then with UMAP, following the default settings of the Seurat package, and were ultimately visualized in a two-dimensional space. Based on the PCA results (Figure S1C), cells were clustered using the SNN algorithm into 24 distinct clusters with similar expression profiles, as visualized in the UMAP plot (*Figure 1A*).

Cell type annotation was performed using the BlueprintEncodeData reference dataset, with subsequent refinement and validation using established marker genes. This process identified eight major cell types: T cells, NK cells, Myeloid cells, B cells, Mast cells, Fibroblasts, Epithelial cells, and Endothelial cells (*Figure 1B*). *Figure 1C,1D* display the characteristic marker genes and the top differential marker genes for each cell type, respectively. Comparative analysis of cell type proportions revealed statistically significant differences between the mLN and tLung groups across all identified types, including epithelial cells (*Figure 1E*).

Significant heterogeneity of epithelial cells in primary and metastatic lung cancer

To elucidate the mechanisms underlying lung cancer metastasis, epithelial cells were further subclustered into 13 distinct subpopulations (EC0–12) (*Figure 2A*). The proportion of these epithelial subpopulations differed significantly between the mLN and tLung groups (*Figure 2B*). Notably, differential abundance analysis revealed that EC2 and EC9 were significantly enriched in mLN samples, while EC0 and EC4–7 were more abundant in tLung samples, suggesting that specific epithelial subpopulations possess an intrinsic predisposition for metastatic dissemination. Pseudotime trajectory analysis of all epithelial cells using Monocle2 indicated a continuum of epithelial differentiation, with clear branching patterns corresponding to distinct cell states (*Figure 2C*). Cells from mLN and tLung showed differential positioning along the trajectory, suggesting tissue-dependent differentiation dynamics. Gene expression heatmaps across pseudotime highlighted dynamic regulation of key epithelial markers (*Figure 2D*), capturing transitions from progenitor-like to more differentiated states. Along the pseudotime trajectory, *ZNF528* expression gradually increased from early to mid-pseudotime and reached its highest level at the distal ends of the right-hand branches (*Figure 2D*). This pattern indicates that *ZNF528* expression is progressively upregulated during the differentiation process and is associated with a late-stage, potentially invasive cellular state.

Differential gene expression analysis between mLN and tLung epithelial populations was performed using the FindMarkers function in Seurat, with results visualized in a volcano plot (*Figure 2E*). Among the 1,002 DEGs identified in epithelial cells, *ZNF528* was notably upregulated in the metastatic (mLN) epithelium, exhibiting a 1.72-fold

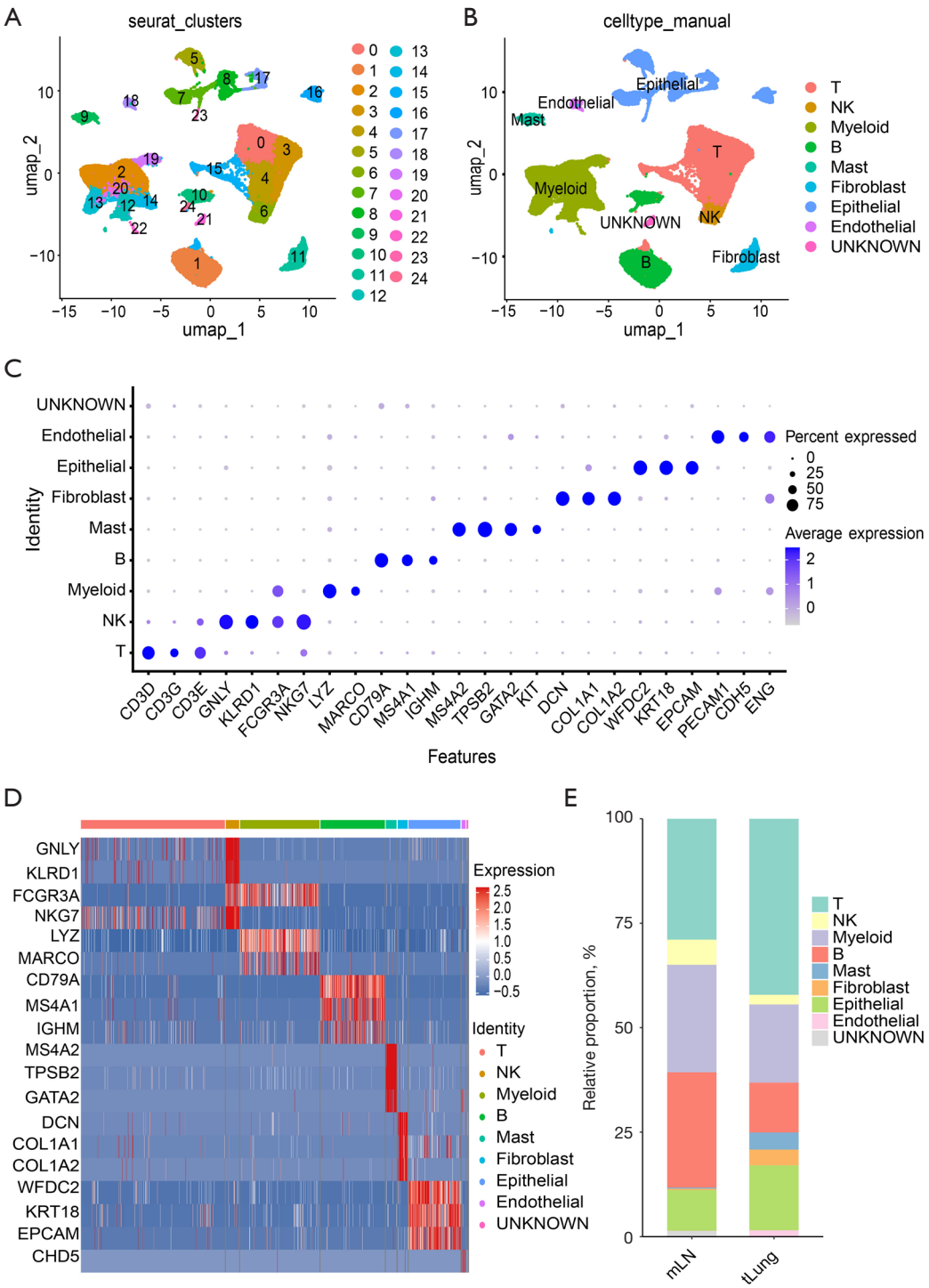

Figure 1 Single-cell transcriptomic landscape of tLung and mLN. (A) UMAP visualisation of 24 distinct clusters identified from all cells. (B) UMAP plot showing annotation of the 24 clusters into nine major cell types. (C) Dot plot depicting the expression levels of canonical marker genes used to define each cell cluster. (D) Heatmap displaying the top differentially expressed marker genes for each annotated cell type. (E) Bar plot showing the relative proportions of each cell subtype in tLung versus mLN groups. mLN, metastatic lymph nodes; tLung, primary lung tumours; UMAP, Uniform Manifold Approximation and Projection.

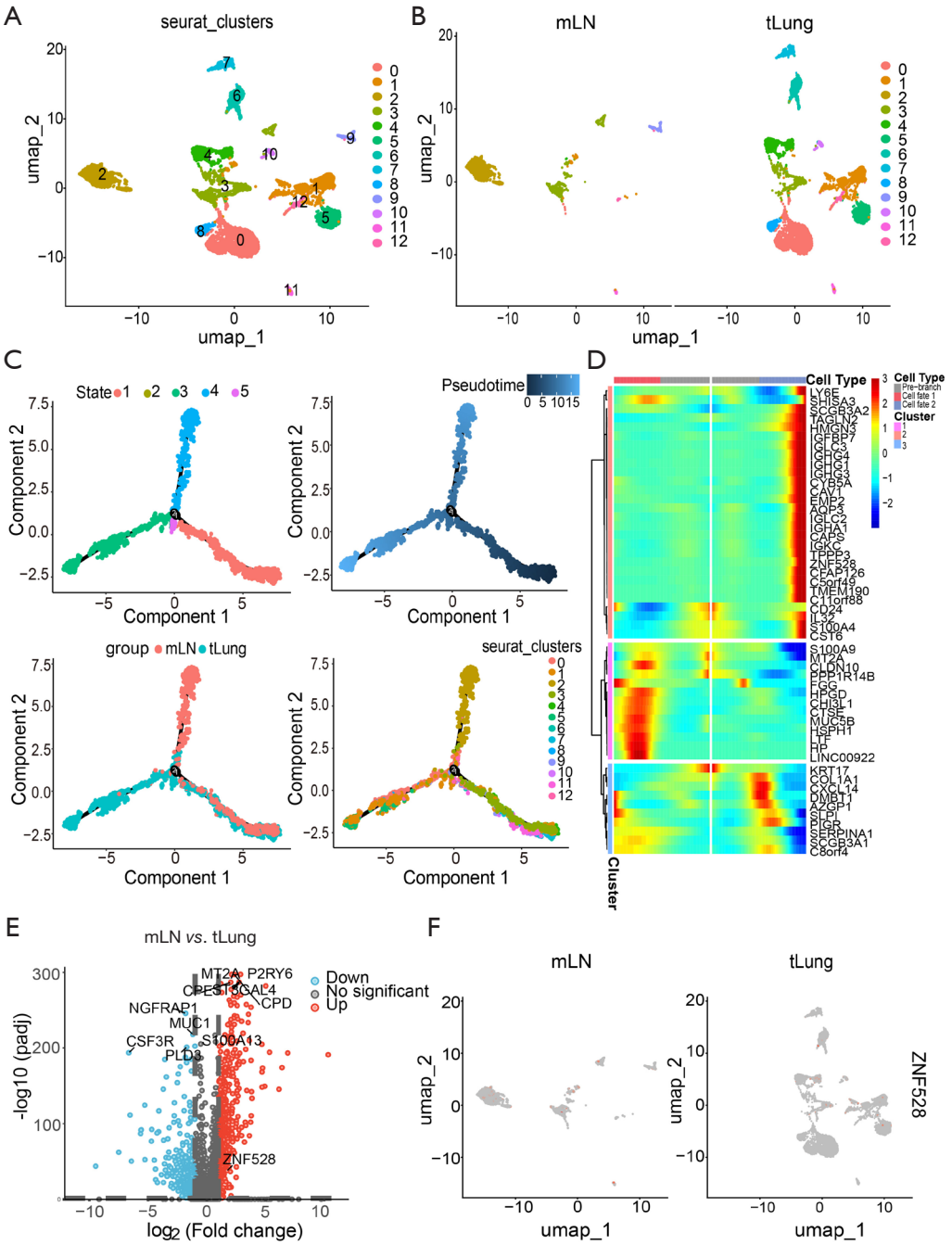

Figure 2 Epithelial cell transcriptional profiles of tLung and mLN groups. (A) UMAP plots of 12 epithelial cell subtypes. (B) UMAP plots of epithelial cell subtypes in the tLung and mLN groups. (C) Pseudotime trajectory analysis of epithelial cells. Top left: cell states colored by inferred differentiation state. Top right: pseudotime progression along the trajectory. Bottom left: cells colored by tissue origin, showing differentiation dynamics in mLN versus tLung. Bottom right: cells colored according to Seurat clusters, highlighting cluster-specific positioning along the trajectory. (D) The heatmap displays expression patterns of selected genes across different cell types and differentiation states during pseudotime analysis. (E) Volcano plot of DEGs in epithelial cells between tLung and mLN groups. Red and blue points indicate significantly up- and down-regulated genes, respectively, with key genes labeled. (F) Distribution of the signature gene *ZNF528* in the epithelial cells of tLung and mLN. DEGs, differentially expressed genes; mLN, metastatic lymph nodes; tLung, primary lung tumours; UMAP, Uniform Manifold Approximation and Projection.

increase in expression (adjusted P=1.49e−38). The expression distribution of *ZNF528* across tLung and mLN epithelial cells is shown in *Figure 2F*, where it was significantly expressed in the EC2 subpopulations within the mLN group, which corresponded precisely to the subpopulations enriched in metastatic samples.

To explore the functional implications of the DEGs in epithelial cells between the two groups, GO and KEGG pathway enrichment analyses were conducted (*Figure 3A,3B*). The results indicated that the significantly upregulated pathways in mLN were closely associated with tumor metastasis, including positive regulation of the MAPK cascade, positive regulation of NF-κB transcription factor activity, TNF signaling pathway, IL-17 signaling pathway, and pyrimidine metabolism. GSEA further confirmed significant upregulation of the pyrimidine metabolism and IL-17 signaling pathways (*Figure 3C,3D*). These findings collectively suggest that epithelial cell heterogeneity plays a pivotal role in the metastatic progression of lung cancer.

ZNF528 is highly expressed in NSCLC and is associated with poor prognosis

To evaluate the clinical relevance of *ZNF528* in NSCLC, based on the GSE31210 database, we first analyzed its prognostic value using K-M survival analysis. As shown in *Figure 4A*, patients with high *ZNF528* expression exhibited significantly shorter overall survival compared to those with low *ZNF528* expression, indicating that *ZNF528* upregulation is associated with poor clinical outcome.

IHC staining was performed to detect *ZNF528* protein levels in clinical primary tumor tissues and adjacent non-tumor tissues. *Figure 4B* demonstrates that *ZNF528* expression was markedly elevated in tumor tissues relative to adjacent normal counterparts. Among 56 NSCLC patients, 18 cases showed low *ZNF528* expression and 38 cases showed high expression. Chi-square analysis further revealed that high *ZNF528* expression was positively correlated with tumor grade (P=0.01) (*Table 1*), suggesting a potential role of *ZNF528* in tumor progression.

We next examined *ZNF528* expression across a panel of NSCLC cell lines. RT-qPCR (*Figure 4C*) and Western blot (*Figure 4D*) analyses showed that, compared with the normal bronchial epithelial cell line BEAS-2B, *ZNF528* mRNA and protein levels were upregulated in both *KRAS*-wild-type (HCC827) and *KRAS*-mutant (A549 and NCI-H358) NSCLC cells. These results indicate that *ZNF528* is upregulated in NSCLC tissues and cell lines, and its high expression correlates with poor prognosis and higher tumor grade.

ZNF528 plays a key role in cell metastasis in vitro

We analyzed LUAD data from the GSE31210, retaining 226 tumor samples for further investigation. Gene sets for the Biocarta p38MAPK, cell cycle, HALLMAPK PI3K AKT MTOR and NF-κappa B pathways were obtained from the MSigDB database, and pathway activity scores for each tumor sample were calculated using the ssgseaParam function in the GSVA package. Using the ggstatsplot package, correlation analysis between *ZNF528* expression and the scores of these pathways showed that *ZNF528* expression was significantly positively associated with key metastasis-related signalling pathways, including Biocarta p38MAPK pathway, Cell cycle, HALLMAPK PI3K AKT MTOR signaling pathway and NF-κappa B signaling pathway (Figure S2A-S2D).

To further define the biological function of *ZNF528* in NSCLC, we established stable *ZNF528* knockdown and overexpressing cell lines in A549 and NCI-H358 cells. The efficiency of *ZNF528* modulation was confirmed at both the mRNA and protein levels by RT-qPCR and Western blot analysis, respectively (*Figure 5A,5B*). CCK-8 assays demonstrated that knockdown of *ZNF528* inhibited the proliferation of A549 and NCI-H358 cells, whereas its overexpression promoted cell proliferation (*Figure 5C*).

The impact of *ZNF528* on NSCLC cell migration and invasion was assessed using wound healing and Transwell assays. The results showed that *ZNF528* knockdown suppressed the migration of both cell lines and showed a trend toward reduced invasion. Conversely, overexpression of *ZNF528* significantly enhanced both the migratory and invasive capacities of A549 and NCI-H358 cells (*Figure 6A,6B*). To investigate the mechanism, we analyzed the expression of EMT-related proteins by Western blot. The results (*Figure 6C*; Figure S3) indicated that *ZNF528* knockdown increased expression of the epithelial marker E-cadherin while decreasing expression of the mesenchymal markers N-cadherin and Vimentin, as well as the EMT transcription factor Snail. Overexpression of *ZNF528* produced the opposite effects, suppressing E-cadherin and elevating N-cadherin, Vimentin, and Snail levels. These data suggest that *ZNF528* promotes EMT progression. Taken together, these results underscore the oncogenic role of *ZNF528* in driving NSCLC cell proliferation, migration, invasion, and EMT.

Given the critical roles of Wnt and Notch signaling

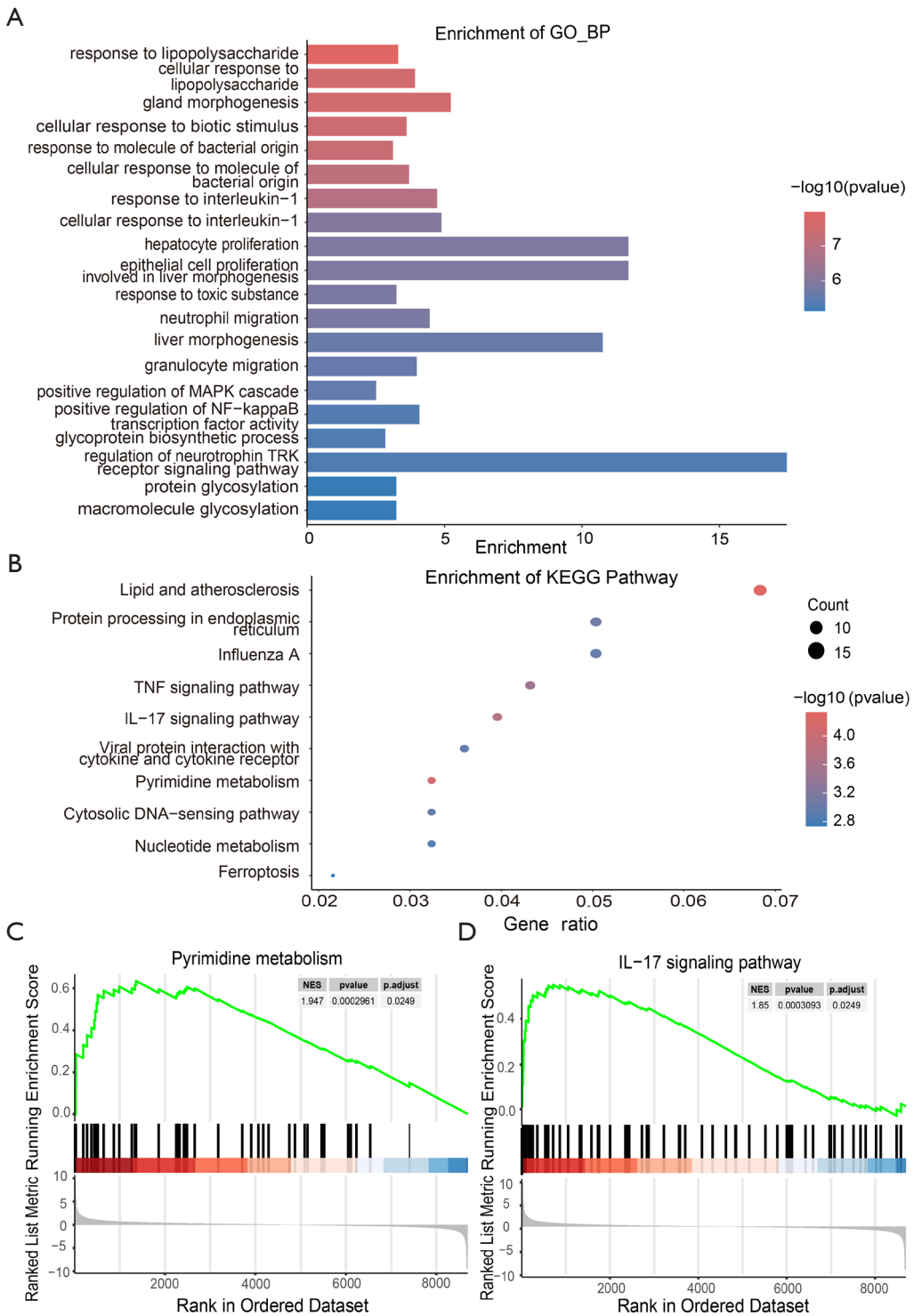

Figure 3 Pathway enrichment analysis of DEGs in epithelial cells between mLN and tLung. (A) Enriched GO-BP terms in mLN versus tLung epithelial cells. (B) Enriched KEGG pathways in mLN versus tLung epithelial cells. (C,D) GSEA enrichment plots for pyrimidine metabolism (C) and IL-17 signalling pathway (D) in mLN epithelial cells. BP, biological process; DEGs, differentially expressed genes; GO, Gene Ontology; GSEA, gene set enrichment analysis; KEGG, Kyoto Encyclopedia of Genes and Genomes; mLN, metastatic lymph nodes; NES, Normalized Enrichment Score; tLung, primary lung tumours.

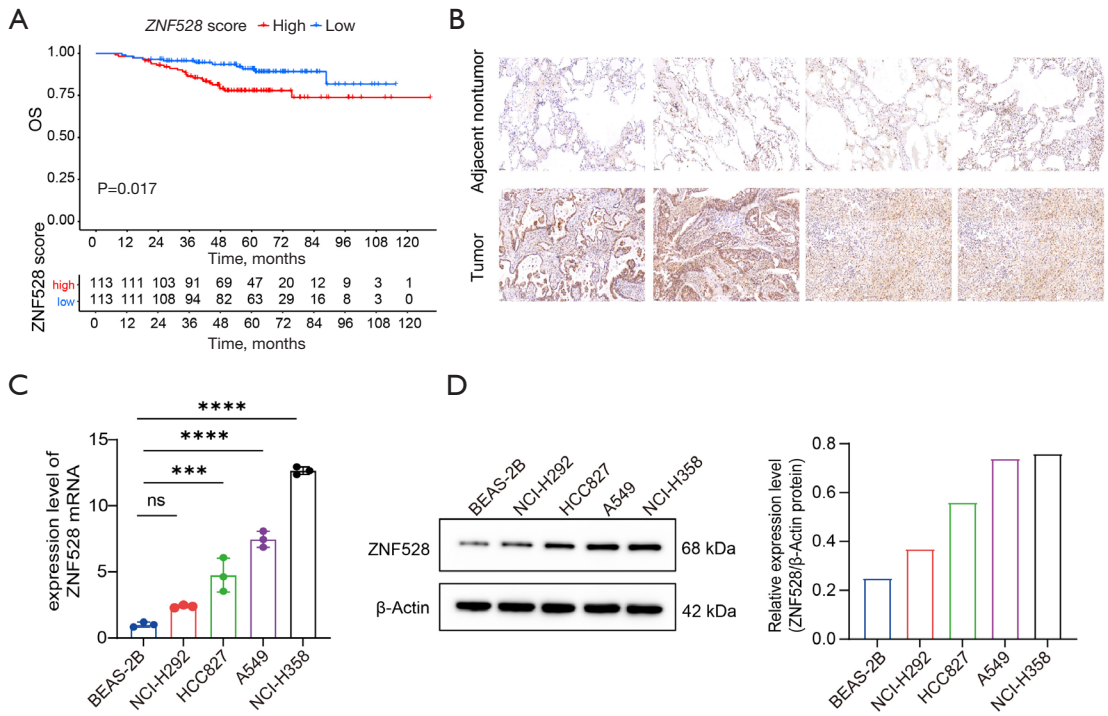

Figure 4 *ZNF528* upregulation correlates with poor prognosis and is elevated in NSCLC tissues and cell lines. (A) Kaplan-Meier survival curves of NSCLC patients with high *vs.* low *ZNF528* expression. (B) IHC staining of *ZNF528* in tumor and adjacent non-tumor tissues (scale bar =50 μm). (C) RT-qPCR analysis of *ZNF528* mRNA levels in the normal bronchial epithelial cell line BEAS-2B and NSCLC cell lines (NCI-H292, HCC827, A549, and NCI-H358). (D) Western blot analysis of *ZNF528* protein expression in the normal bronchial epithelial cell line BEAS-2B and NSCLC cell lines (NCI-H292, HCC827, A549, and NCI-H358). The count was repeated three times and data are represented as the mean ± SD. (ns, P≥0.05; ***, P<0.001; ****, P<0.0001). IHC, immunohistochemical; mRNA, messenger RNA; ns, not significant; NSCLC, non-small cell lung cancer; OS, overall survival; RT-qPCR, reverse transcription quantitative polymerase chain reaction; SD, standard deviation.

pathways in EMT and tumor progression, we next assessed the expression of key components of these pathways. As shown in *Figure 6D* (Figure S4), *ZNF528* overexpression upregulated the protein levels of β-catenin, p-GSK-3β and total GSK-3β in A549 and NCI-H358 cells, indicative of Wnt pathway activation. Additionally, *ZNF528* overexpression elevated the levels of Notch intracellular domain (NICD) and its downstream effector Hes1, demonstrating activation of Notch signaling. In contrast, *ZNF528* knockdown suppressed the expression of these pathway mediators.

ZNF528 promotes migration, invasion, and EMT in NSCLC cells via SNAIL regulation

To investigate the functional role of *ZNF528* in NSCLC progression, gain-of-function experiments combined with *SNAIL* knockdown were performed in A549 and NCI-H358 cells. Wound healing assays demonstrated that overexpression of *ZNF528* significantly enhanced the migratory capacity of both A549 and NCI-H358 cells compared to control groups. However, silencing of SNAIL markedly attenuated the promotive effect of *ZNF528* on cell migration (*Figure 7A,7B*). Consistently, Transwell migration assays further confirmed that *ZNF528* overexpression led to a significant increase in the number of migrated cells, whereas *SNAIL* knockdown partially reversed this effect (*Figure 7C,7D*). Similarly, Transwell invasion assays showed that *ZNF528* significantly promoted the invasive ability of NSCLC cells, while *SNAIL* depletion suppressed *ZNF528*-induced invasion (*Figure 7E,7F*).

At the molecular level, Western blot analysis revealed that *ZNF528* overexpression decreased the expression of the epithelial marker E-cadherin and increased the expression

Table 1 Association between *ZNF528* expression levels and clinicopathological features in patients

Clinicopathological features	ZNF528 low expression (n=18)	ZNF528 high expression(n=38)	χ^2 value	P value	Statistical significance
Gender			0.394	0.53	Not significant
Male	12 (66.7)	22 (57.9)			
Female	6 (33.3)	16 (42.1)			
Age group			0.296	0.59	Not significant
<60 years	8 (44.4)	14 (36.8)			
≥60 years	10 (55.6)	24 (63.2)			
Grade			6.31	0.01*	Significant
1–2	11 (61.1)	10 (26.3)			
3	7 (38.9)	28 (73.7)			
Distant metastasis			1.651	0.20	Not significant
No	17 (94.4)	31 (81.6)			
Yes	1 (5.6)	7 (18.4)			
Lymph node metastasis			0.823	0.36	Not significant
No	16 (88.9)	30 (78.9)			
Yes	2 (11.1)	8 (21.1)			

Data are presented as n (%). *, P<0.05.

of mesenchymal markers N-cadherin and Vimentin, along with upregulation of *SNAIL*. Notably, knockdown of *SNAIL* reversed these EMT-related changes induced by *ZNF528* (*Figure 7G*,*7H*).

Collectively, these results indicate that *ZNF528* promotes migration, invasion, and epithelial-mesenchymal transition in NSCLC cells, at least in part through a SNAIL-dependent mechanism.

Upregulation of ZNF528 promotes lung cancer growth and metastasis in vivo

To assess the impact of *ZNF528* on NSCLC growth *in vivo*, nude mice were subcutaneously inoculated with NSCLC cells overexpressing *ZNF528*. Tumor volume was monitored every three days beginning on day 10. At the experimental endpoint (day 28), mice were euthanized, and tumors were excised and photographed. Overexpression of *ZNF528* significantly enhanced tumor growth compared to the control group (*Figure 8A-8C*). Western blot analysis confirmed higher *ZNF528* protein expression in tumors from the *ZNF528*-overexpressing group (*Figure 8D*, Figure S3). Consistent with *in vitro* observations, *ZNF528*-overexpressing tumors displayed reduced levels of the epithelial marker E-cadherin, along with elevated expression of the mesenchymal markers N-cadherin and Vimentin, and the transcription factor Snail, indicating that *ZNF528* promotes EMT *in vivo* (*Figure 8D*). Histopathological examination further revealed extensive proliferative lesions in subcutaneous tumors from the *ZNF528* overexpression group (*Figure 8E*).

In the Luc-LLC experimental lung metastasis model, mice injected with *ZNF528*-overexpressing cells exhibited significantly stronger bioluminescent signals in the lungs compared to the control group, indicating enhanced metastatic burden (*Figure 8F*). Upon termination of the experiment, visual inspection and quantitative analysis revealed a marked increase in the number of metastatic nodules on the lung surfaces in the *ZNF528* overexpression group (*Figure 8G*,*8H*). Histological assessment confirmed prominent tumor formation in these lungs. Furthermore, IHC staining demonstrated significantly elevated *ZNF528* protein expression within the metastatic tumors of the

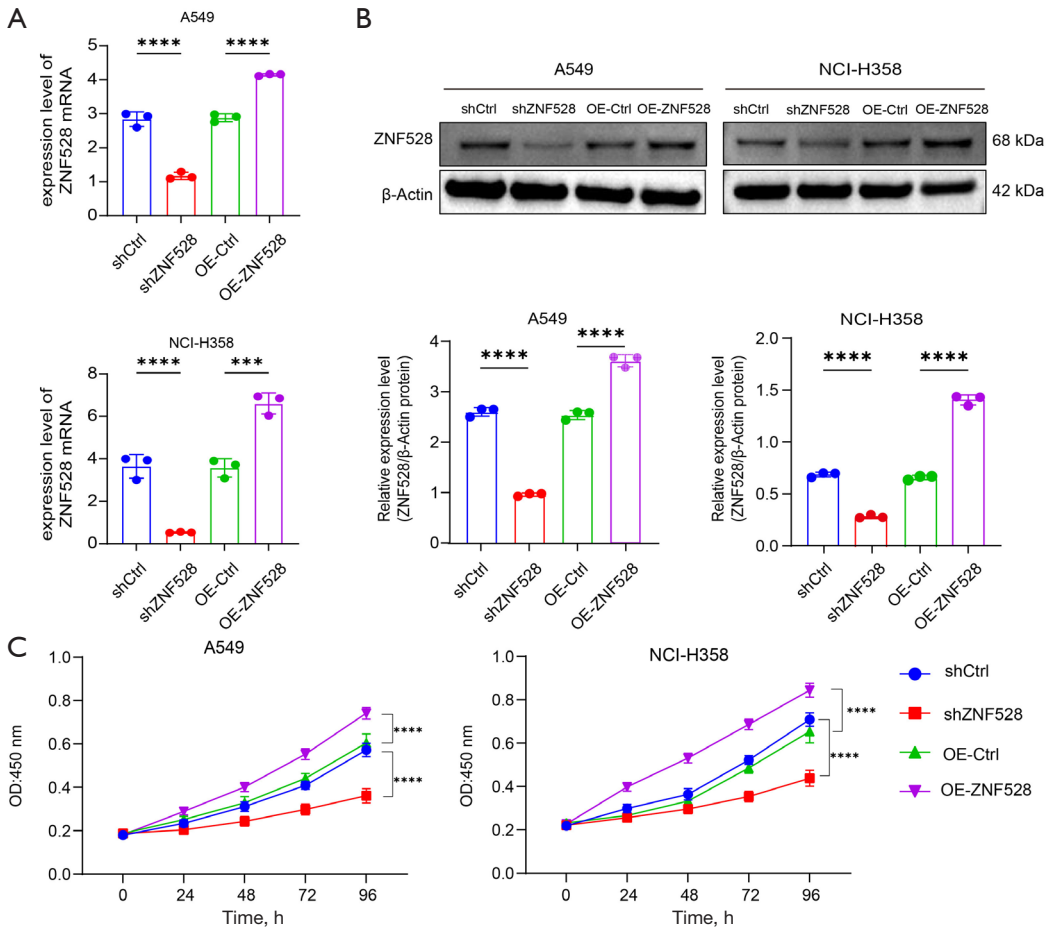

Figure 5 *ZNF528* promoted the proliferation of NSCLC cells. (A) The efficiency of *ZNF528* knockdown and overexpression in A549 and NCI-H358 cells was detected by RT-qPCR following transfection. (B) The efficiency of *ZNF528* knockdown and overexpression in A549 and NCI-H358 cells was confirmed by Western blot. Protein intensity was analyzed by densitometry, and the levels were normalized to β-actin. (C) Cell proliferation was assessed using the CCK-8 assay in A549 and NCI-H358 cells after *ZNF528* knockdown or overexpression. The count was repeated three times and data are represented as the mean ± SD. (***, P<0.001; ****, P<0.0001). CCK-8, Cell Counting Kit-8; mRNA, messenger RNA; NSCLC, non-small cell lung cancer; OD, optical density; RT-qPCR, reverse transcription quantitative polymerase chain reaction; SD, standard deviation.

ZNF528-overexpressing group (*Figure 8I*).

Discussion

In this study, we employed scRNA-seq to investigate the mechanisms underlying lung cancer metastasis. Through analysis of the GEO database, we identified DEGs in epithelial cells from primary and metastatic lung cancer tissues, among which *ZNF528* was markedly upregulated in the metastatic epithelium. Subsequent *in vitro* and *in vivo* experiments demonstrated that *ZNF528* promotes lung cancer cell migration and invasion by facilitating EMT. Our findings suggest that *ZNF528* may serve as a prognostic indicator for lung cancer metastasis and represent a promising therapeutic target for metastatic NSCLC.

NSCLC constitutes approximately 85% of all lung cancer cases. Despite advances in clinical management—including surgery, chemotherapy, radiotherapy, and immunotherapy—NSCLC remains highly metastatic, resulting in a 5-year survival rate of only 10–20% (4,17). Metastasis is the leading cause of lung cancer-related mortality, involving a complex interplay of multiple signaling pathways and cellular functions. Nevertheless, the molecular mechanisms driving lung cancer metastasis are still not fully understood.

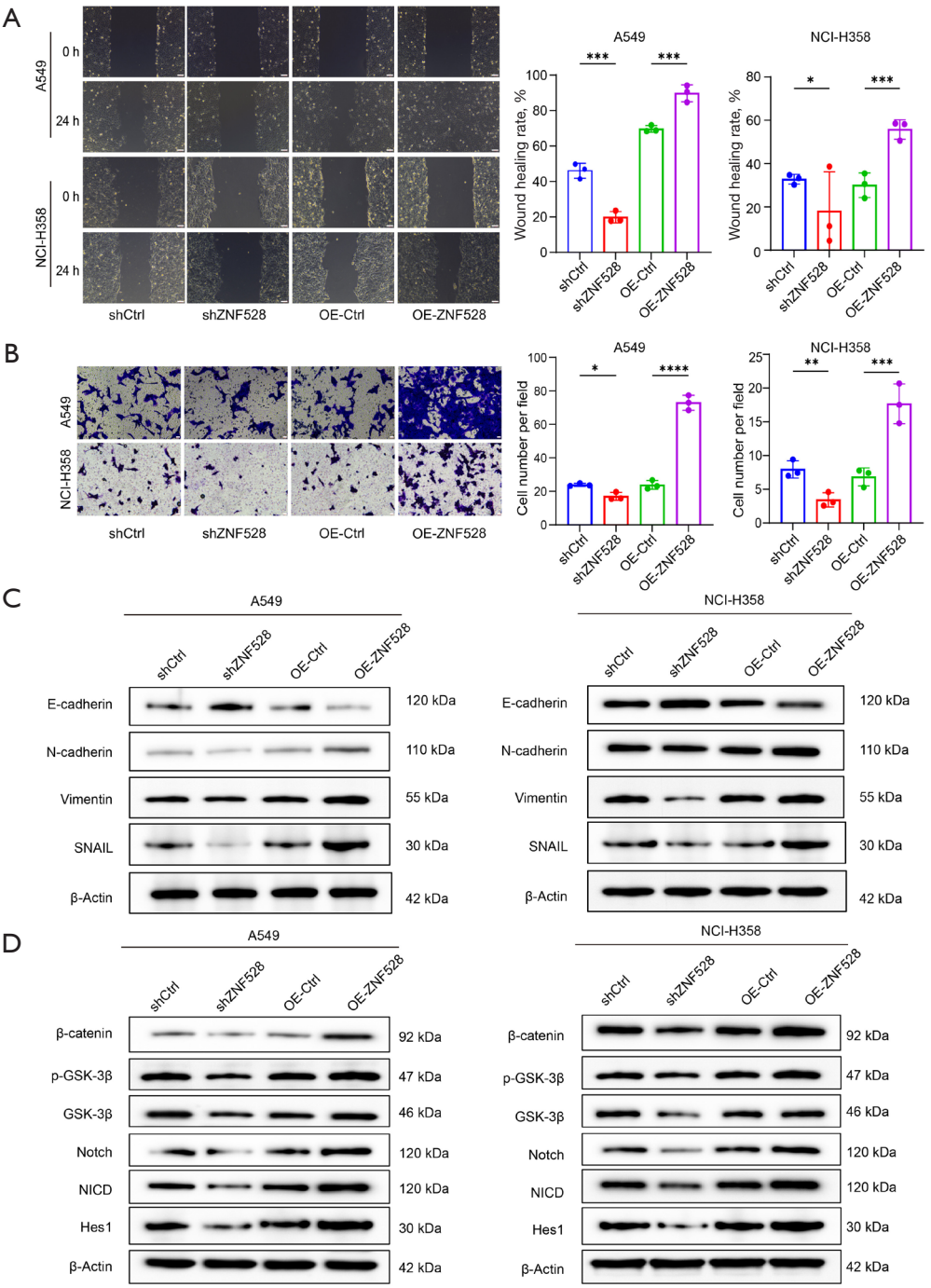

Figure 6 *ZNF528* promoted migration and invasion of NSCLC cells. (A) Cell migration ability was assessed by wound healing assay in A549 and NCI-H358 cells following *ZNF528* knockdown or overexpression (scale bar =100 μm). (B) Cell invasion capacity was evaluated using Transwell assay in A549 and NCI-H358 cells after *ZNF528* knockdown or overexpression (scale bar =30 μm, crystal violet stained). (C) Protein levels of E-cadherin, N-cadherin, Vimentin, SNAIL, and β-Actin were detected by Western blot in A549 and NCI-H358 cells following *ZNF528* knockdown or overexpression. (D) Protein levels of β-catenin, p-GSK-3β, GSK-3β, Notch, NICD, Hes1, and β-Actin were detected by Western blot in A549 and NCI-H358 cells following *ZNF528* knockdown or overexpression. The count was repeated three times and data are represented as the mean ± SD. (*, P<0.05; **, P<0.01; ***, P<0.001; ****, P<0.0001). NICD, Notch intracellular domain; NSCLC, non-small cell lung cancer; OE, overexpression; SD, standard deviation.

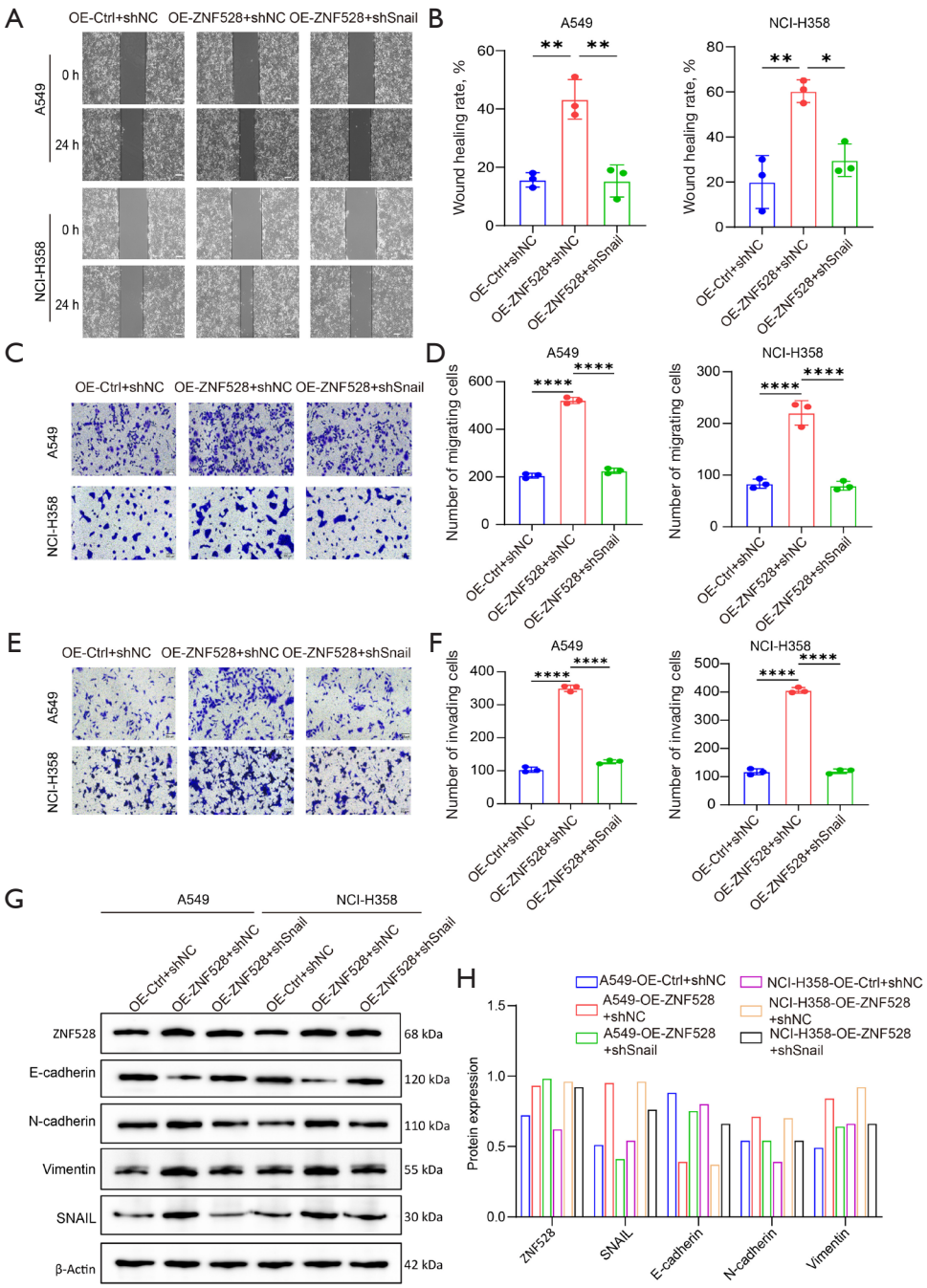

Figure 7 *ZNF528* promotes migration, invasion, and EMT in NSCLC cells via SNAIL regulation. (A,B) Cell migration ability was assessed by wound healing assay in A549 and NCI-H358 cells following *ZNF528* overexpression, or *ZNF528* overexpression with SNAIL knockdown (scale bar =100 μm). (C,D) Cell migration capacity was evaluated using Transwell assay in A549 and NCI-H358 cells after *ZNF528* overexpression, or *ZNF528* overexpression with SNAIL knockdown (scale bar =30 μm, crystal violet stained). (E,F) Cell invasion capacity was evaluated using Transwell assay in A549 and NCI-H358 cells after *ZNF528* overexpression, or *ZNF528* overexpression with SNAIL knockdown (scale bar =30 μm, crystal violet stained). (G,H) Protein levels of *ZNF528*, E-cadherin, N-cadherin, Vimentin, SNAIL, and β-Actin were detected by Western blot in A549 and NCI-H358 cells following *ZNF528* overexpression, or *ZNF528* overexpression with SNAIL knockdown. The count was repeated three times and data are represented as the mean ± SD. (*, P<0.05; **, P<0.01; ****, P<0.0001). EMT, epithelial-mesenchymal transition; NSCLC, non-small cell lung cancer; OE, overexpression; SD, standard deviation.

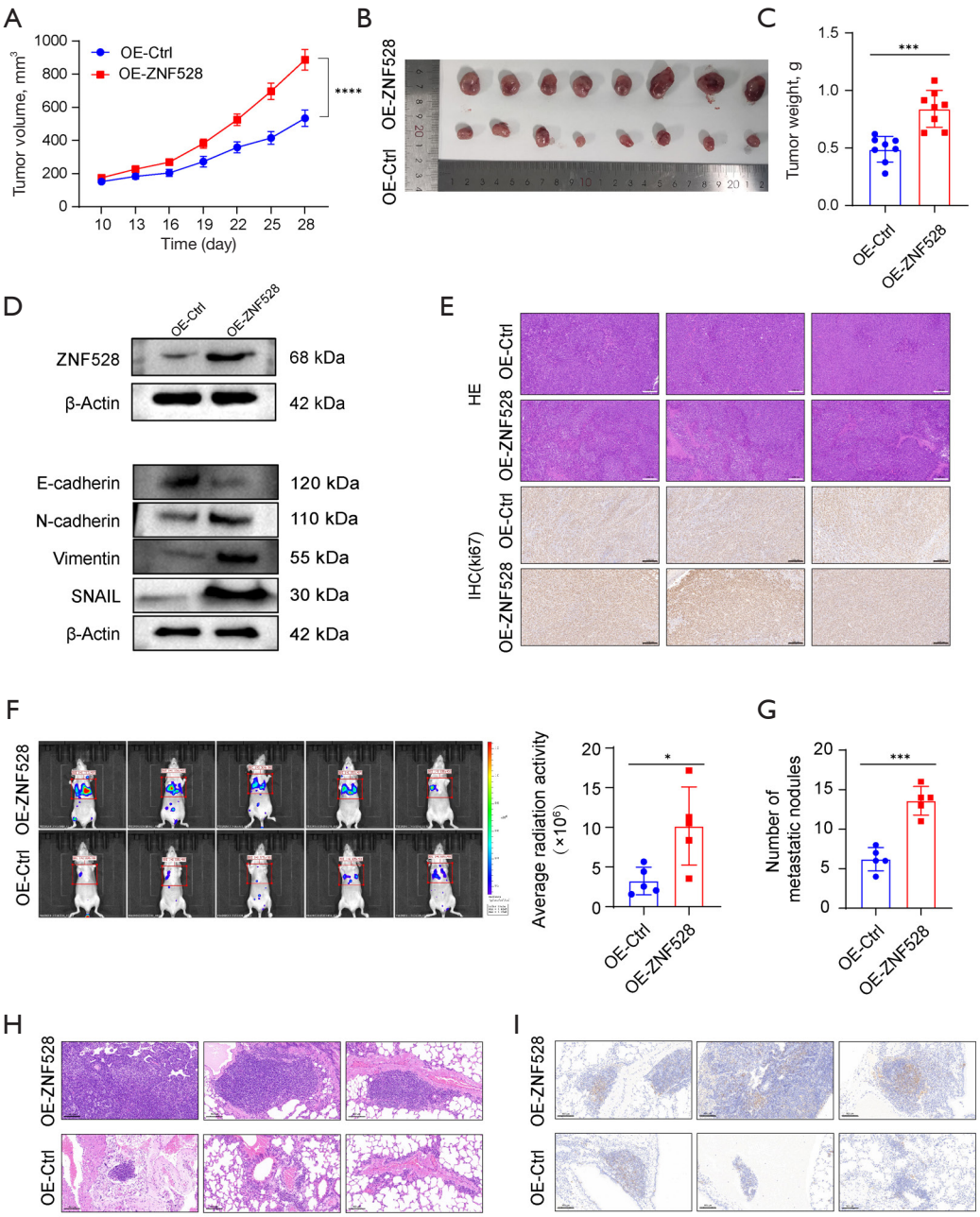

Figure 8 *ZNF528* overexpression promotes NSCLC growth and metastasis *in vivo*. (A) Monitoring of tumor volume in nude mice following subcutaneous inoculation of A549 cells. (B) Representative photographs of excised tumors from each group at the experimental endpoint. (C) Quantification of tumor weight. (D) Western blot analysis of *ZNF528*, E-cadherin, N-cadherin, Vimentin, and SNAIL protein expression in tumor tissues from the control and *ZNF528*-overexpressing groups; β-Actin served as the loading control. (E) Histological evaluation of tumor tissues by HE staining and IHC staining for Ki67 (scale bar =200 μm). (F) *In vivo* bioluminescence imaging and quantification of metastatic burden in mice after tail-vein injection of Luc-LLC cells. (G) Quantitative analysis of metastatic lung nodules. H&E staining (H) and IHC staining (I) for *ZNF528* in lung tissues from the control and *ZNF528*-overexpressing groups (scale bar =100 μm). Data are presented as mean ± SD. (***, P<0.001; ****, P<0.0001). HE, hematoxylin and eosin; IHC, immunohistochemical; Luc-LLC, luciferase-labeled mouse Lewis lung carcinoma; NSCLC, non-small cell lung cancer; OE, overexpression.

In the present study, analysis of single-cell transcriptomic data from primary and lymphatically metastatic lung cancer tissues revealed elevated expression of *ZNF528* in epithelial cells from metastatic lesions. Validation in an independent scRNA-seq cohort would be needed to confirm the robustness of these findings across samples. *ZNF528* belongs to the KRAB C2H2 zinc-finger protein family, yet its biological function in cancer remains largely unexplored. Our GSEA and KEGG analyses revealed that pathways such as MAPK cascade, NF-κB transcription factor activity, IL-17 signalling, TNF signalling and pyrimidine metabolism were significantly upregulated in mLN epithelial cells compared to tLung cells. The association of these pathways with tumour metastasis is well documented. Dysregulated MAPK signalling is known to promote NSCLC progression through regulation of proliferation, differentiation and EMT (18). NF-κB activation enhances metastasis by inducing EMT, a mechanism confirmed in lung cancer among other tumour types (19). IL-17 signalling has been reported to promote migration, invasion and EMT in lung cancer cells (20). TNF family members play important roles in oncogenesis and progression (21), and pyrimidine metabolism has been recognised as a hallmark of cancer that promotes tumour advancement (22). Together, these pathway-level findings support the functional relevance of our single-cell analyses. Our functional assays demonstrated that knockdown of *ZNF528* suppressed NSCLC cell migration and invasion, whereas its overexpression enhanced these malignant phenotypes, suggesting that *ZNF528* acts as a tumor-promoting factor in NSCLC metastasis.

EMT is a phenotypic reprogramming process that confers loss of epithelial characteristics and acquisition of mesenchymal traits, thereby enhancing cell motility and invasiveness (18,19). Metastatic cancer cells hijack the EMT program to initiate dissemination, and aberrant EMT activation is closely associated with cancer stemness and therapy resistance (23-25). EMT is regulated by a complex network of signaling pathways, including TGF-β, Wnt/β-catenin, and Notch, which converge on key transcription factors such as TWIST1, SNAI1/2, and ZEB1/2 (26-28). In the present study, immunoblot analysis of *ZNF528*-knockdown and *ZNF528*-overexpressing NSCLC cells revealed that *ZNF528* overexpression promotes the expression of mesenchymal markers (N-cadherin and vimentin) and the EMT-inducing transcription factor SNAIL, while suppressing the epithelial marker E-cadherin. Given the critical roles of Wnt and Notch signaling pathways in EMT, we examined the expression of proteins involved in these pathways under different *ZNF528* expression levels in NSCLC cells and found that *ZNF528* promotes EMT through activation of both Wnt and Notch signaling. *SNAIL* is a well-established driver of tumour metastasis that represses E-cadherin expression and facilitates the EMT process (29,30). By knocking down SNAIL in *ZNF528*-overexpressing NSCLC cells, we observed that SNAIL depletion reversed the *ZNF528*-promoted migration and invasion of tumor cells, indicating that *ZNF528* regulates NSCLC migration and invasion at least partially through SNAIL. Collectively, these findings suggest that pharmacological inhibition of Wnt or Notch signaling may abrogate *ZNF528*-driven EMT and metastatic phenotypes, providing a rationale for targeting these pathways as a therapeutic strategy in *ZNF528*-overexpressing NSCLC.

Most KRAB-containing zinc-finger proteins (KRAB-ZFPs) function as transcriptional repressors through recruitment of KAP1. However, an increasing number of KRAB-ZFPs have been reported to act as transcriptional activators depending on cellular context or the presence of specific co-factors. *ZNF528*, while containing a KRAB domain, promoted the expression of SNAIL and mesenchymal markers in our study, suggesting an activating function. This is not without precedent; for example, ZNF71 has been shown to promote EMT in NSCLC (31), and other KRAB-ZFPs have been implicated in transcriptional activation via context-dependent mechanisms (32). The precise molecular basis for *ZNF528*'s activating role, whether through loss of KAP1 interaction, recruitment of co-activators, or indirect effects, remains to be elucidated and warrants further investigation.

Our study provides evidence that *ZNF528* promotes lung cancer metastasis through EMT activation. Nevertheless, several limitations should be acknowledged. First, we used two *KRAS*-mutant NSCLC lines: A549 (adenocarcinoma, *KRAS* G12S) and H358 (bronchioloalveolar carcinoma, *KRAS* G12C). Although their distinct histological and biological backgrounds may contribute to baseline differences in EMT marker expression or drug responsiveness, *ZNF528* consistently promoted migration, invasion and EMT in both lines, supporting a robust pro-metastatic function that is largely independent of cellular context. We did not formally dissect the contribution of cell line heterogeneity to the observed phenotypes; this warrants future investigation using isogenic models. Our functional studies were conducted exclusively in LUAD-derived cell lines (A549 and H358). Whether *ZNF528* exerts similar

pro-metastatic effects in other NSCLC subtypes, such as squamous cell carcinoma, remains unknown and warrants future investigation using a broader panel of cell lines. Second, the *in vivo* assessment of *ZNF528*'s pro-metastatic function relied primarily on the tail vein injection model. This model bypasses early steps of the metastatic cascade, including local invasion and intravasation, and primarily measures circulating survival and colonisation capacity rather than spontaneous haematogenous metastasis. More importantly, it evaluates haematogenous dissemination, whereas our single-cell data suggest a potential role for *ZNF528* in lymphatic metastasis. Whether *ZNF528* specifically promotes lymphatic spread, haematogenous spread, or both therefore remains unknown. Future studies using orthotopic or spontaneous metastasis models with lymphatic tracing are needed to dissect its pathway-specific functions. Third, as our *in vivo* studies were performed in immunodeficient mice, the potential role of *ZNF528* in modulating the tumour-immune microenvironment, a critical determinant of metastatic progression, remains an important avenue for future investigation. Fourth, the clinical relevance of our findings would be strengthened by correlating *ZNF528* expression with clinicopathological parameters—such as tumor-node-metastasis (TNM) stage, metastasis-free survival, and overall survival—in a large NSCLC patient cohort. Finally, a prospective power analysis was not performed to determine the sample size for our *in vivo* experiments (n=6 per group). While this sample size is consistent with standard practice in the field for xenograft and tail vein metastasis models, and our key endpoints demonstrated statistically significant differences, the absence of a formal power calculation may be considered a limitation. Future studies should include a prospective power analysis to ensure adequate statistical power for detecting predefined effect sizes.

Beyond the limitations noted above, the potential therapeutic relevance of our findings warrants further consideration. Zoledronic acid inhibits the mevalonate pathway, blocking prenylation of small G proteins (Ras, Rac, Rho) (33) and reversing EMT via JAK/STAT3 (34) suppression. As *ZNF528* promotes EMT, zoledronic acid might antagonise this effect. Denosumab, an anti-RANKL antibody, reduces NSCLC migration and invasion through NF-κB and MEK/ERK downregulation (35,36). Notably, *KRAS*-mutant H358 cells are relatively resistant to zoledronic acid alone (33); however, combining it with a KRAS G12C inhibitor could be synergistic. Similarly, in A549 cells (*KRAS* G12S), combining zoledronic acid with MEK or pan-RAS inhibitors may enhance anti-metastatic efficacy. While these hypotheses are beyond the current scope, they provide a strong rationale for future studies in *ZNF528*-overexpressing models.

Conclusions

In conclusion, this multi-faceted study utilized single-cell transcriptomics to identify epithelial cells as a critical niche in metastatic NSCLC and to uncover *ZNF528* as a key driver of malignancy. We provide compelling functional evidence that *ZNF528* promotes NSCLC cell migration, invasion, and metastasis. These findings establish *ZNF528* as a novel oncogene in NSCLC progression and highlight its potential as a therapeutic target against metastatic disease.

Acknowledgments

None.

Footnote

Reporting Checklist: The authors have completed the ARRIVE and MDAR reporting checklists. Available at https://tlcr.amegroups.com/article/view/10.21037/tlcr-2026-1-0008/rc

Data Sharing Statement: Available at https://tlcr.amegroups.com/article/view/10.21037/tlcr-2026-1-0008/dss

Peer Review File: Available at https://tlcr.amegroups.com/article/view/10.21037/tlcr-2026-1-0008/prf

Funding: This study was supported by the National Natural Science Foundation of China Young Scientists Fund (No. 82304567), the National Natural Science Foundation of China (No. 82073367), Jiangsu Provincial Research Hospital (No. YJXYY202204-2-ZD03), Nanjing Health Technology Development Project (No. YKK23106), Jiangsu Province Aging Health Research Project (No. LKZ2023013), the Cadre Health Care Project of Jiangsu Province (No. BJ2408), and New Technology Development Project of Nanjing Drum Tower Hospital (No. XJSFZLX202454).

Conflicts of Interest: All authors have completed the ICMJE uniform disclosure form (available at https://tlcr.amegroups.com/article/view/10.21037/tlcr-2026-1-0008/coif). All authors report receiving funding from the National Natural

Science Foundation of China, Jiangsu Provincial Research Hospital, Nanjing Health Technology Development Project, Jiangsu Province Aging Health Research Project, Cadre Health Care Project of Jiangsu Province, and New Technology Development Project of Nanjing Drum Tower Hospital. The authors have no other conflicts of interest to declare.

Ethical Statement: The authors are accountable for all aspects of the work in ensuring that questions related to the accuracy or integrity of any part of the work are appropriately investigated and resolved. The study was conducted in accordance with the Declaration of Helsinki and its subsequent amendments. This study was approved by the Ethics Committee of Nanjing Drum Tower Hospital (Approval No. 263-02), and written informed consent was obtained from all patients prior to sample collection. Experiments were performed under a project license (Approval No. 263-02) granted by the Ethics Committee of Nanjing Drum Tower Hospital, in compliance with institutional guidelines for the care and use of animals.

References

1. Bray F, Laversanne M, Sung H, et al. Global cancer statistics 2022: GLOBOCAN estimates of incidence and mortality worldwide for 36 cancers in 185 countries. CA Cancer J Clin 2024;74:229-63.
2. Thai AA, Solomon BJ, Sequist LV, et al. Lung cancer. Lancet 2021;398:535-54.
3. Schneegans S, Löptien J, Mojzisch A, et al. HERC5 downregulation in non-small cell lung cancer is associated with altered energy metabolism and metastasis. J Exp Clin Cancer Res 2024;43:110.
4. Sun Y, Chen D, Sun S, et al. RBMS1 Coordinates with the m6A Reader YTHDF1 to Promote NSCLC Metastasis through Stimulating S100P Translation. Adv Sci (Weinh) 2024;11:e2307122.
5. Schmitges FW, Radovani E, Najafabadi HS, et al. Multiparameter functional diversity of human C2H2 zinc finger proteins. Genome Res 2016;26:1742-52.
6. Urrutia R. KRAB-containing zinc-finger repressor proteins. Genome Biol 2003;4:231.
7. Lupo A, Cesaro E, Montano G, et al. KRAB-Zinc Finger Proteins: A Repressor Family Displaying Multiple Biological Functions. Curr Genomics 2013;14:268-78.
8. Wolfe SA, Nekludova L, Pabo CO. DNA recognition by Cys2His2 zinc finger proteins. Annu Rev Biophys Biomol Struct 2000;29:183-212.
9. Najafabadi HS, Mnaimneh S, Schmitges FW, et al. C2H2 zinc finger proteins greatly expand the human regulatory lexicon. Nat Biotechnol 2015;33:555-62.
10. Tan W, Zheng L, Lee WH, et al. Functional dissection of transcription factor ZBRK1 reveals zinc fingers with dual roles in DNA-binding and BRCA1-dependent transcriptional repression. J Biol Chem 2004;279:6576-87.
11. Skarp S, Xia JH, Zhang Q, et al. Exome Sequencing Reveals a Phenotype Modifying Variant in ZNF528 in Primary Osteoporosis With a COL1A2 Deletion. J Bone Miner Res 2020;35:2381-92.
12. Zhang J, Guo H, Gong C, et al. Therapeutic targets in the Wnt signaling pathway: Treating cancer with specificity. Biochem Pharmacol 2025;236:116848.
13. Du X, Luo W, Li H, et al. Hsa_circ_0125356 promotes gemcitabine resistance by modulating WNT canonical and non-canonical pathways via miR-582-5p/FGF9 axis in non-small cell lung cancer. Mol Cancer 2025;24:59.
14. Hong CL, Yu IS, Pai CH, et al. CD248 Regulates Wnt Signaling in Pericytes to Promote Angiogenesis and Tumor Growth in Lung Cancer. Cancer Res 2022;82:3734-50.
15. Huo Y, Xu X, Ma X, et al. GINS1 Enhances Glycolysis, Proliferation and Metastasis in Lung Adenocarcinoma Cells by Activating the Notch/PI3K/AKT/mTORC1 Signaling Pathway. Zhongguo Fei Ai Za Zhi 2024;27:735-44.
16. Wang Y, Chen P, Zhao M, et al. EGFL7 drives the evolution of resistance to EGFR inhibitors in lung cancer by activating NOTCH signaling. Cell Death Dis 2022;13:910.
17. Riely GJ, Wood DE, Ettinger DS, et al. Non-Small Cell Lung Cancer, Version 4.2024, NCCN Clinical Practice Guidelines in Oncology. J Natl Compr Canc Netw 2024;22:249-74.
18. Wu L, Yu M, Liang H, et al. SJB2-043, a USP1 Inhibitor, Suppresses A549 Cell Proliferation, Migration, and EMT via Modulation of PI3K/AKT/mTOR, MAPK, and Wnt

Signaling Pathways. Curr Issues Mol Biol 2025;47:155.
19. Mirzaei S, Saghari S, Bassiri F, et al. NF-κB as a regulator of cancer metastasis and therapy response: A focus on epithelial-mesenchymal transition. J Cell Physiol 2022;237:2770-95.
20. Liu W, Xin M, Li Q, et al. IL-17A Promotes the Migration, Invasion and the EMT Process of Lung Cancer Accompanied by NLRP3 Activation. Biomed Res Int 2022;2022:7841279.
21. Li J, Chen B, Huang Y, et al. TNF-α modulates cell proliferation via SOX4/TGF-β/Smad signaling in benign prostatic hyperplasia. Cell Death Dis 2025;16:472.
22. Luo Y, Tian W, Lu X, et al. Prognosis stratification in breast cancer and characterization of immunosuppressive microenvironment through a pyrimidine metabolism-related signature. Front Immunol 2022;13:1056680.
23. Singh A, Settleman J. EMT, cancer stem cells and drug resistance: an emerging axis of evil in the war on cancer. Oncogene 2010;29:4741-51.
24. Shibue T, Weinberg RA. EMT, CSCs, and drug resistance: the mechanistic link and clinical implications. Nat Rev Clin Oncol 2017;14:611-29.
25. Dakal TC, Bhushan R, Xu C, et al. Intricate relationship between cancer stemness, metastasis, and drug resistance. MedComm (2020) 2024;5:e710.
26. Bagby M, Greener EH. Infrared spectral kinetic analysis of EBA-HV-ZnO cements. Dent Mater 1985;1:89-92.
27. Xue W, Yang L, Chen C, et al. Wnt/β-catenin-driven EMT regulation in human cancers. Cell Mol Life Sci 2024;81:79.
28. Feng M, Santhanam RK, Xing H, et al. Inhibition of γ-secretase/Notch pathway as a potential therapy for reversing cancer drug resistance. Biochem Pharmacol 2024;220:115991.
29. Jacob S, Ahluwalia C, Chintamani C. Expression of EMT Markers Snail, Slug, and Twist and their Association with Known Prognostic Indicators of Breast Cancer. Indian J Surg Oncol 2024;15:706-12.
30. Bao Z, Zeng W, Zhang D, et al. SNAIL Induces EMT and Lung Metastasis of Tumours Secreting CXCL2 to Promote the Invasion of M2-Type Immunosuppressed Macrophages in Colorectal Cancer. Int J Biol Sci 2022;18:2867-81.
31. Ye Q, Mohamed R, Dakhlallah D, et al. Molecular Analysis of ZNF71 KRAB in Non-Small-Cell Lung Cancer. Int J Mol Sci 2021;22:3752.
32. Sobocińska J, Molenda S, Machnik M, et al. KRAB-ZFP Transcriptional Regulators Acting as Oncogenes and Tumor Suppressors: An Overview. Int J Mol Sci 2021;22:2212.
33. Kenessey I, Kói K, Horváth O, et al. KRAS-mutation status dependent effect of zoledronic acid in human non-small cell cancer preclinical models. Oncotarget 2016;7:79503-14.
34. Yang X, Gao Y, Liu Q, et al. Zoledronic acid re-sensitises gefitinib-resistant lung cancer cells by inhibiting the JAK/STAT3 signalling pathway and reversing epithelial-mesenchymal transition. Oncol Rep 2021;45:459-68.
35. De Castro J, García R, Garrido P, et al. Therapeutic Potential of Denosumab in Patients With Lung Cancer: Beyond Prevention of Skeletal Complications. Clin Lung Cancer 2015;16:431-46.
36. Dai X, Xia H, Zhou S, et al. Zoledronic acid enhances the efficacy of the MEK inhibitor trametinib in KRAS mutant cancers. Cancer Lett 2019;442:202-12.

Cite this article as: Li H, Lin Y, Wang Y, Chen X, Xie Y, Yu T, He J, Yin Z, Xia M. *ZNF528* as a novel driver of metastasis in lung cancer: insights from single-cell transcriptomics. Transl Lung Cancer Res 2026;15(5):119. doi: 10.21037/tlcr-2026-1-0008